Supplementary Text

S1 On priors and updates to the WASP model

The WASP model described in Goodwin (2018) is used here, with updated prior distributions, functional forms of radiative forcing from greenhouse gasses and aerosols and internal noise in the energy imbalance. The random-normal prior distribution for the Planck feedback,λ_{Planck} (Supplementary Table 1), is estimated via $\lambda_{Planck} = 4f\sigma T^3$, where f is the greenhouse fraction of upwards longwave radiation at the top of the atmosphere relative to the surface (Trenberth et al., 2014), σ is the Stephan-Boltzmann constant and T is the global mean surface temperature of Earth (Jones and Hapham, 2013). Use uniform prior probability distributions for λ_{fast} (from -3.0 to +1.0 $Wm^{-2}K^{-1}$) and λ_{slow} (from -3.0 to +2.0 $Wm^{-2}K^{-1}$).

The random-normal prior distribution for the CO_2 radiative forcing coefficient (Supplementary Table 1) is taken from the estimate of IPCC (2013), $a_{CO2} = 5.35 \pm 0.27$ Wm^{-2}. The functional forms of radiative forcing from CH_4 and N_2O are updated after Etminan et al. (2016), with random-normal prior distributions of uncertainty (Supplementary Table 1) to reflect uncertainty for these relations estimated in Etminan et al. (2016). A radiative forcing term is introduced to WASP here to represent the internal variability in Earth's energy imbalance using AR1 noise, with the constants tuned to imposed monthly and annual root-mean-square energy imbalance after Trenberth et al. (2014).

S2 Radiative forcing from aerosols in the WASP model

The calculation of radiative forcing from aerosols in the WASP model (Goodwin, 2016) is updated in this study. The version of WASP described in Goodwin (2018) uses a single time series for aerosol radiative forcing scaled by a single uncertainty parameter that is varied between ensemble members. Here, aerosol radiative forcing is separated into direct and indirect aerosol forcing components from emissions of different types of aerosols: Black Carbon (BC), Organic Carbon (OC), sulphates (SO_x), nitrous oxides (NO_X), ammonia (NH_3) and volatile organic compounds (VOC).

The version of WASP used here is updated to employ aerosol radiative forcing based on the FAIR v1.3 (Smith et al., 2018) model scheme, with this scheme chosen as it avoids the use of iterative computational methods and thus retains computational efficiency. The direct aerosol radiative forcing over time is related to the emissions of different anthropogenic aerosol types, E_x, via

$$R_{dir-aero}(t) = \gamma_{aero-BC}E_{BC} + \gamma_{aero-OC}E_{OC} + \gamma_{aero-SO_x}E_{SO_x} + \gamma_{aero-NO_x}E_{NO_x} + \gamma_{aero-NH_3}E_{NH_3} + \gamma_{aero-VOC}E_{VOC} \quad \text{(S1)}$$

which assumes anthropogenic aerosol are sufficiently short-lived in the atmosphere such that radiative forcing can be related directly to emissions without an intermediate step of calculating atmospheric concentrations (Smith et al., 2018).

The AeroCom experiments (Myhre et al., 2013) analyse direct radiative forcing for each aerosol type across multiple atmospheric models in the year 2010. Smith et al. (2018) uses these 2010 best estimates (Myhre et al., 2013) to constrain the coefficients $\gamma_{aero-BC}$, $\gamma_{aero-OC}$, $\gamma_{aero-SO_x}$, $\gamma_{aero-NO_x}$, $\gamma_{aero-NH_3}$ and $\gamma_{aero-SOA}$ in the FaIR model. In the WASP model used here, this is extended by using the uncertainty estimates in Myhre et al. (2013) to independently vary the values of coefficients $\gamma_{aero-BC}$, $\gamma_{aero-OC}$, $\gamma_{aero-SO_x}$, $\gamma_{aero-NO_x}$, $\gamma_{aero-NH_3}$ and $\gamma_{aero-VOC}$ between the prior ensemble members (Supplementary Table 1). Thus, the prior WASP ensemble here is representative of the multi-model variation in how sensitive direct aerosol radiative forcing is to emissions of each aerosol type evaluated in Myhre et al. (2013).

The coefficients relating aerosol emissions to direct radiative forcing are thus written (Supplementary Table S1): $\gamma_{aero-SO_x} = (-0.32 \pm 0.11)/E_{SO_x-2010}$; $\gamma_{aero-BC} = (0.18 \pm 0.07)/E_{BC-2010}$; $\gamma_{aero-OC} = (-0.03 \pm 0.01)/E_{OC-2010}$; and $\gamma_{aero-VOC} = (-0.06 \pm 0.09)/E_{VOC-2010}$. Nitrate aerosol radiative forcing is split into components of 40% from NO_X and 60% from NH_3, as used by Smith et al. (2018), giving: $\gamma_{NO_x} = 0.4 \times (-0.08 \pm 0.04)/E_{NO_x-2010}$; and $\gamma_{NH_3} = 0.6 \times (-0.08 \pm 0.04)/E_{NH_3-2010}$.

WASP is also updated to use an emulation of indirect aerosol radiative forcing from aerosol-cloud interaction, $R_{aci}(t)$ in Wm^{-2}, after FaIRv.13 model (Smith et al., 2018),

$$R_{aci}(t) = -R_{aci:2011}\frac{G(t) - G(t_{1765})}{G(t_{2011}) - G(t_{1765})} \quad \text{(S2)}$$

where $R_{aci:2011}$ is the radiative forcing from aerosol cloud interaction in 2011, and G is related to emissions of aerosol components via *(sign check below)*;

$$G(t) = -1.95\log\left(1 + 0.0111E_{SO_x}(t) + 0.0139[E_{OC}(t) + E_{BC}(t)]\right) \quad \text{(S3)}$$

We vary the value of $R_{aci:2011}$ between the prior ensemble members to account for the skewed uncertainty in indirect aerosol radiative forcing estimated within IPCC AR5 (IPCC, 2013). To account for a skew in the uncertainty in historic indirect aerosol radiative forcing (IPCC, 2013), a skewed-normal prior distribution for $R_{aci:2011}$ is adopted (Supplementary Table S1).

Supplementary References

Andrews T., Gregory J.M., Webb M.J.: The dependence of radiative forcing and feedback on evolving patterns of surface temperature change in climate models. J Clim 28:1630–1648. https://doi.org/10.1175/JCLI-D-14-00545.1, 2015.

Cheng, L., Trenberth, K.E., Fasullo, J., Boyer, T., Abraham, J., Zhu, J.: Improved estimates of ocean heat content from 1960 to 2015. Science Advances, 3, 3, e1601545, https://doi.org/10.1126/sciadv.1601545, 2017.

Etminan, M., Myhre, G., Highwood, E.J., Shine, K.P.: Radiative forcing of carbon dioxide, methane, and nitrous oxide: A significant revision of the methane radiative forcing, Geophys. Res. Lett., 43, 12,614–12,623, https://doi:10.1002/2016GL071930, 2016.

Fine, R. A., Peacock, S., Maltrud, M. E., & Bryan, F. O.: A new look at ocean ventilation time scales and their uncertainties. Journal of Geophysical Research: Oceans, 122, 3771–3798. https://doi.org/10.1002/2016JC012529, 2017.

Goodwin, P.: On the time evolution of climate sensitivity and future warming. Earth's Future 6, EFT2466, https://doi.org/10.1029/2018EF000889, 2018.

Gregory, J.M., Andrews, T., Good, P., Mauritsen, T., Forster, P.M.: Small global-mean cooling due to volcanic radiative forcing. Climate Dynamics, 47, 3979-3991, https://doi.org/10.1007/s00382-016-3055-1, 2016.

IPCC: Climate Change 2013: The Physical Science Basis. Contribution of Working Group 1 to the Fifth Assessment Report of the Intergovernmental Panel on Climate Change In T. F. Stocker, et al. (Eds.). (1535 pp.). Cambridge, UK: Cambridge University Press. https://doi.org/10.1017/CBO9781107415324, 2013.

Jones, P. D., Harpham, C., Estimation of the absolute surface air temperature of the Earth. J. Geophys. Res. Atmos., 118, 3213–3217, https://doi.org/10.1002/jgrd.50359, 2013.

Kennedy J.J., Rayner, N.A., Smith, R.O., Saunby, M. and Parker, D.E.: Reassessing biases and other uncertainties in sea-surface temperature observations since 1850 part 1: measurement and sampling errors. J. Geophys. Res., 116, D14103, https://doi.org/10.1029/2010JD015218, 2011.

le Quéré, C., Andrew, R. M., Friedlingstein, P., Sitch, S., Hauck, J., Pongratz, J., Pickers, P. A., Korsbakken, J. I., Peters, G. P., Canadell, J. G., Arneth, A., Arora, V. K., Barbero, L., Bastos, A., Bopp, L., Chevallier, F., Chini, L. P., Ciais, P.,

Doney, S. C., Gkritzalis, T., Goll, D. S., Harris, I., Haverd, V., Hoffman, F. M., Hoppema, M., Houghton, R. A., Hurtt, G., Ilyina, T., Jain, A. K., Johannessen, T., Jones, C. D., Kato, E., Keeling, R. F., Goldewijk, K. K., Landschützer, P., Lefèvre, N., Lienert, S., Liu, Z., Lombardozzi, D., Metzl, N., Munro, D. R., Nabel, J. E. M. S., Nakaoka, S., Neill, C., Olsen, A., Ono, T., Patra, P., Peregon, A., Peters, W., Peylin, P., Pfeil, B., Pierrot, D., Poulter, B., Rehder, G., Resplandy, L., Robertson, E., Rocher, M., Rödenbeck, C., Schuster, U., Schwinger, J., Séférian, R., Skjelvan, I., Steinhoff, T., Sutton, A., Tans, P. P., Tian, H., Tilbrook, B., Tubiello, F. N., van der Laan-Luijkx, I. T., van der Werf, G. R., Viovy, N., Walker, A. P., Wiltshire, A. J., Wright, R., Zaehle, S., and Zheng, B.: Global Carbon Budget 2018, Earth Syst. Sci. Data, 10, 2141–2194, https://doi.org/10.5194/essd-10-2141-2018, 2018.

Levitus, S., Antonov, J.I., Boyer, T.P., Baranova, O.K., Garcia, H.E., Locarnini, R.A., Mishonov, A.V., Reagan, J.R., Seidov, D., Yarosh, E.S. and Zweng, M.M.: World ocean heat content and thermosteric sea levelchange (0–2000 m), 1955–2010. Geophysical Research Letters, 39, https://doi.org/10.1029/2012GL051106, 2012.

Morice, C.P., Kennedy, J.J., Rayner, N.A. and Jones, P.D.: Quantifying uncertainties in global and regional temperature change using an ensemble of observational estimates: the HadCRUT4 dataset. Journal of Geophysical Research, 117, D08101, https://doi.org/10.1029/2011JD017187, 2012

Myhre, G., Samset, B. H., Schulz, M., Balkanski, Y., Bauer, S., Berntsen, T. K., Bian, H., Bellouin, N., Chin, M., Diehl, T., Easter, R. C., Feichter, J., Ghan, S. J., Hauglustaine, D., Iversen, T., Kinne, S., Kirkevåg, A., Lamarque, J.-F., Lin, G., Liu, X., Lund, M. T., Luo, G., Ma, X., van Noije, T., Penner, J. E., Rasch, P. J., Ruiz, A., Seland, Ø., Skeie, R. B., Stier, P., Takemura, T., Tsigaridis, K., Wang, P., Wang, Z., Xu, L., Yu, H., Yu, F., Yoon, J.-H., Zhang, K., Zhang, H., and Zhou, C.: Radiative forcing of the direct aerosol effect from AeroCom Phase II simulations, Atmos. Chem. Phys., 13, 1853–1877, https://doi.org/10.5194/acp-13-1853-2013, 2013.

Trenberth, K.E., Fasullo, J.T., and Balmaseda, M.A.: Earth's Energy Imbalance, Journal of Climate, 27, 3129-3144. https://doi.org/10.1175/JCLI-D-13-00294.1, 2014.

van der Ent, R. J., Tuinenburg, O. A.: The residence time of water in the atmosphere revisited. Hydrology and Earth System Sciences, 21, 779–790. https://doi.org/10.5194/hess-21-779-2017, 2017.

Supplementary Tables:

Model input parameter	**Prior Distribution**	**Notes**
λ_{Planck}, Planck climate feedback	Normal, μ= 3.2 Wm^{-2}; σ = 0.2 Wm^{-2}	Estimated from global energy budget (Trenberth et al., 2014) and global mean temperature (Jones and Harpham, 2013).
λ_{Fast}^{equil}, climate feedback from fast processes at equilibrium	Uniform, min. = -3.0 Wm^{-2}, max. = +1.0 Wm^{-2}	Assume equal prior likelihood from -3.0 to +1.0 Wm^{-2}
τ_{Fast}, e-folding timescale of fast climate feedback processes	Normal, μ =8.9 days , σ = 0.4 days	Set to residence timescale for water vapour in the atmosphere (van der Ent and Tuinenberg, 2017)
λ_{Slow}^{equil}, climate feedback from slow processes at equilibrium	Uniform, min. = -3.0 Wm^{-2}, max. = +2.0 Wm^{-2}.	Assume equal prior likelihood from -3.0 to +2.0 Wm^{-2}
τ_{Slow}, e-folding timescale of slow climate feedback processes	Uniform, min. = 20 years, max. = 45 years	Linked to the minimum time window over which slow climate feedbacks are evaluated (20 years) in climate models by Andrews et al. (2015) and the ventilation timescale of the upper thermocline (45 years) identified by Fine et al. (2017).
a_{CO2}, the radiative forcing coefficient for a log change in CO_2	Normal, μ = 5.35 Wm^{-2}, σ = 0.27 Wm^{-2}	IPCC (2013)
Dimensionless uncertainty in N_2O radiative forcing	Normal, μ = 1.0, σ = 0.05.	To represent percentage uncertainty of Etminan et al. (2016)
Dimensionless uncertainty in CH_4 radiative forcing	Normal, μ = 1.0, σ = 0.07.	To represent percentage uncertainty of Etminan et al. (2016)

Dimensionless uncertainty in Halocarbon radiative forcing	Normal, μ = 1.0, σ = 0.05.	To represent percentage uncertainty of Myhre et al. (2013)
Coefficient of radiative forcing from volcanic aerosols	Normal, μ = -19.0 Wm^{-2}, σ = -0.5 Wm^{-2}.	Relates volcanic AOD to radiative forcing after Gregory et al. (2016)
Radiative forcing from SO_X aerosols in 2010, $\gamma_{SO_x} E_{SO_x}$	Normal, μ = -0.31 Wm^{-2}, σ = 0.11 Wm^{-2}	From AeroCom experiment, Myhre et al. (2013)
Radiative forcing from Black Carbon (BC) aerosols in 2010, $\gamma_{BC} E_{BC}$	Normal, μ = 0.18 Wm^{-2}, σ = 0.07 Wm^{-2}	From AeroCom experiment, Myhre et al. (2013)
Radiative forcing from Nitrous Oxide (NO_X) aerosols in 2010, $\gamma_{NO_x} E_{NO_x}$	Normal, μ = -0.032 Wm^{-2}, σ = 0.016 Wm^{-2}	From AeroCom experiment, Myhre et al. (2013) with 40% weighting
Radiative forcing from Volatile Organic Compound (NMVOC) aerosols in 2010, $\gamma_{SOA} E_{NMVOC}$	Normal, μ = -0.06 Wm^{-2}, σ = 0.09 Wm^{-2}	From AeroCom experiment, Myhre et al. (2013)
Radiative forcing from Organic Carbon (OC) aerosols in 2010, $\gamma_{OC} E_{OC}$	Normal, μ = -0.03 Wm^{-2}, σ = 0.01 Wm^{-2}	From AeroCom experiment, Myhre et al. (2013)
Radiative forcing from NH_3 aerosols in 2010, $\gamma_{NH_3} E_{NH_3}$	Normal, μ = -0.048 Wm^{-2}, σ = 0.024 Wm^{-2}	From AeroCom experiment, Myhre et al. (2013)
The radiative forcing from indirect aerosol effects in 2010, $-R_{aci:2011}$	Skew-normal, μ = -0.55 Wm^{-2}, σ = 0.37 Wm^{-2}, skew = -2.0.	To approximate indirect aerosol radiative forcing distribution of AR5 (IPCC., 2013).
Carbon exchange e-folding timescale between atmosphere and surface ocean mixed layer	Uniform, min. = 0.5 yrs, max. = 1.0 yrs	As used in WASP prior ensemble of Goodwin (2018).
Tracer exchange e-folding timescale surface ocean mixed layer to upper thermocline	Uniform, min. = 5 yrs, max. = 40 yrs	

Tracer exchange e-folding timescale surface ocean mixed layer to intermediate water	Uniform, min. = 15 yrs, max. = 60 yrs
Tracer exchange e-folding timescale surface ocean mixed layer to deep water	Uniform, min. = 100 yrs, max. = 500 yrs
Tracer exchange e-folding timescale surface ocean mixed layer to bottom water	Uniform, min. = 400 yrs, max. = 1500 yrs
The atmosphere-ocean buffered carbon inventory, I_b	Uniform, min. = 3100 PgC, max. = 3500 PgC
Ratio of surface warming global near surface to global sea surface at equilibrium	Uniform, min. = 0.20, max. = 1.5
Ratio of global whole-ocean warming to global sea surface warming at equilibrium	Uniform, min. = 0.1, max. = 1.0

Supplementary Table S1: Prior distributions of the 25 varied model input parameters.

Historic observational constraint	**Mean and standard deviation of likelihood used for the ensembles**	
Surface warming anomalies, relative to 1961-1990 baseline	***HadCRUT4 ensembles***	***Cowtan&Way ensembles***
ΔT during 1850-1899	μ = -0.314 °C; σ = 0.084 °C.	μ = -0.351 °C; σ = 0.058 °C.
ΔT during 1900-1919	μ = -0.388 °C; σ = 0.066 °C.	μ = -0.378 °C; σ = 0.043 °C.
ΔT during 1920-1939	μ = -0.178 °C; σ = 0.057 °C.	μ = -0.168 °C; σ = 0.031 °C.
ΔT during 1940-1959	μ = 0.034 °C; σ = 0.053 °C.	μ = -0.021 °C; σ = 0.028 °C.
ΔT during 1960-1979	μ = -0.066 °C; σ = 0.042 °C.	μ = -0.061 °C; σ = 0.016 °C.
ΔT during 1980-1999	μ = 0.185 °C; σ = 0.043 °C.	μ = 0.190 °C; σ = 0.021 °C.
ΔT during 2000-2019	μ = 0.537 °C; σ = 0.045 °C.	μ = 0.577 °C; σ = 0.030 °C.
SST anomaly relative to 1961-1990	***All ensembles*** **(HadSST3)**	
ΔSST during 1850-1899	μ = -0.276 °C, σ = 0.076 °C	
Heat content anomaly	***Cheng et al. ensembles***	***NODC ensembles***
ΔOHC upper 700m, 1960-1969 to 2006-2015	$\mu = 75.6\times10^{21}$ J; $\sigma = 12.3\times10^{21}$ J	-
ΔOHC from 700m to 2000m, 1960-1969 to 2006-2015	$\mu = 177.8\times10^{21}$ J; $\sigma = 13.8\times10^{21}$ J	-
ΔOHC for whole ocean, 1960-1969 to 2006-2015	$\mu = 360\times10^{21}$ J; $\sigma = 35\times10^{21}$ J	-
ΔOHC upper 700m, from 1955-1959 to 2015-2019	-	$\mu = 211.9\times10^{21}$ J; $\sigma = 18.5\times10^{21}$ J
ΔOHC upper 2000m, from 1955-1959 to 2015-2019	-	$\mu = 314.5\times10^{21}$ J; $\sigma = 20.3\times10^{21}$ J
Total Earth System heat content anomaly, 1971 to 2010	-	$\mu = 274\times10^{21}$ J; $\sigma = 48\times10^{21}$ J

Ocean carbon uptake	***All ensembles (Global Carbon Budget)***
Whole ocean carbon content increase, 1982 to start of 2018	μ= 71.2 PgC, σ= 24.3 PgC

Supplementary Table S2: Historic likelihood distributions applied as constraints to extract the posterior ensemble from the prior ensemble. Quantities are derived from observational-reconstruction datasets HadCRUT4 (Morice et al., 2012); Cowtan&Way v2 (Cowtan & Way, 2014); NODC (Levitus et al., 2012); Cheng et al. (2017); HadSST3.1 (Kennedy et al., 2011); and the Global Carbon Budget (le Quéré et al., 2018). The mean values (μ) for each multi-year average quantity (aside from NODC) are calculated as the time-average of the annual means for the relevant period. NODC already provides the 5-year time average. The standard deviation (σ) is provided by over the relevant 5-year time-period for the NODC dataset, while σ in the ocean carbon budget refers to an instantaneous cumulative change and is calculated from the 2 times the standard deviation of observation-constrained ocean models used within the Global Carbon Budget (le Quéré et al., 2018); where we multiply the standard deviation of the observation-constrained models by 2 since this small sample of 7 models may not be dispersive enough to capture the full uncertainty in ocean carbon uptake. For all other datasets where a multi-year time average is used, the value of σ for the time-average periods considered is estimated as the time-average of the annual values of σ. In the HadCRUT4 dataset the annual σ is assumed to be given by the annual 95% range in temperature anomaly divided by 4. This method of estimating the multi-year time-average from annual values of σ is equivalent to assuming perfect correlation between where the true value lies within the uncertainty distribution from one year to the next, and provides a larger value of σ for the relevant time-period than assumptions involving reduced correlation.

Supplementary Figures:

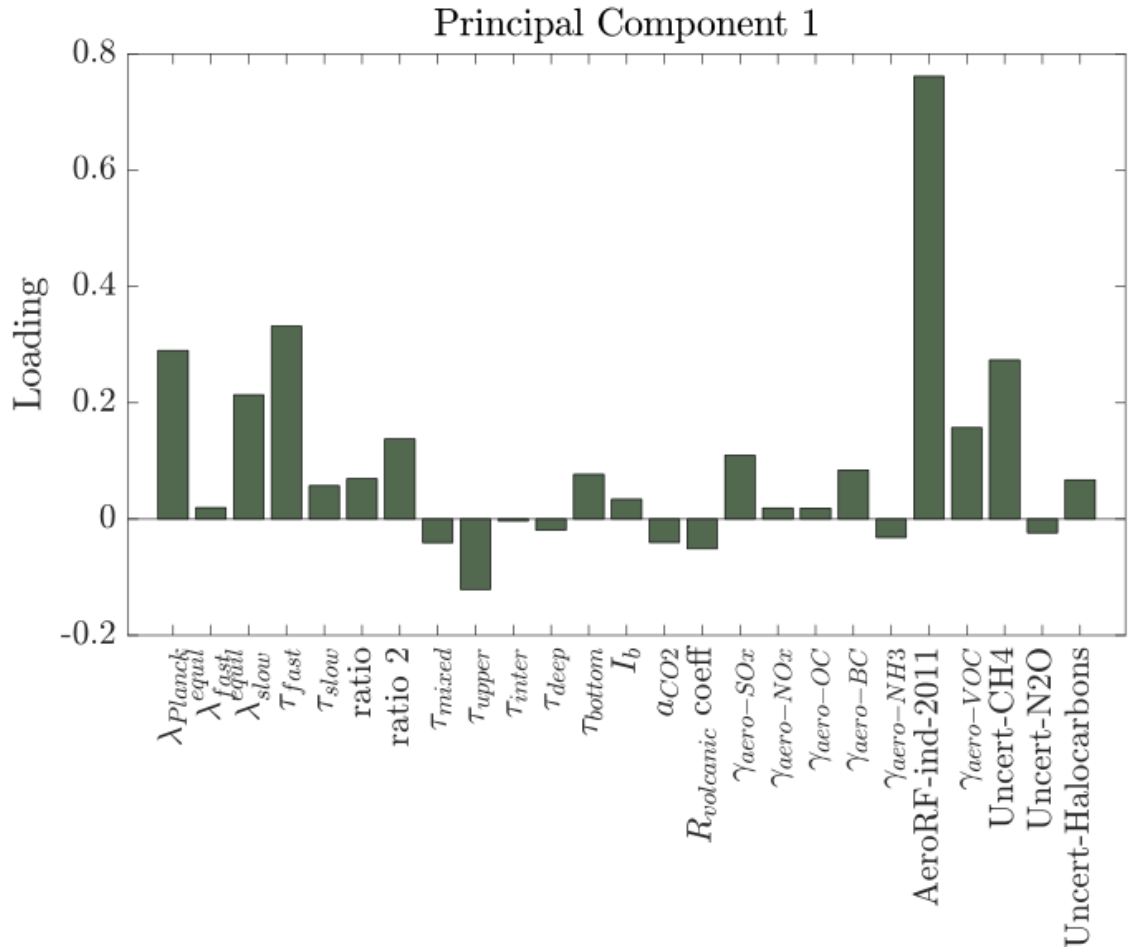

Figure S1. Principle component 1 of the varied model parameters within the posterior model ensembles.

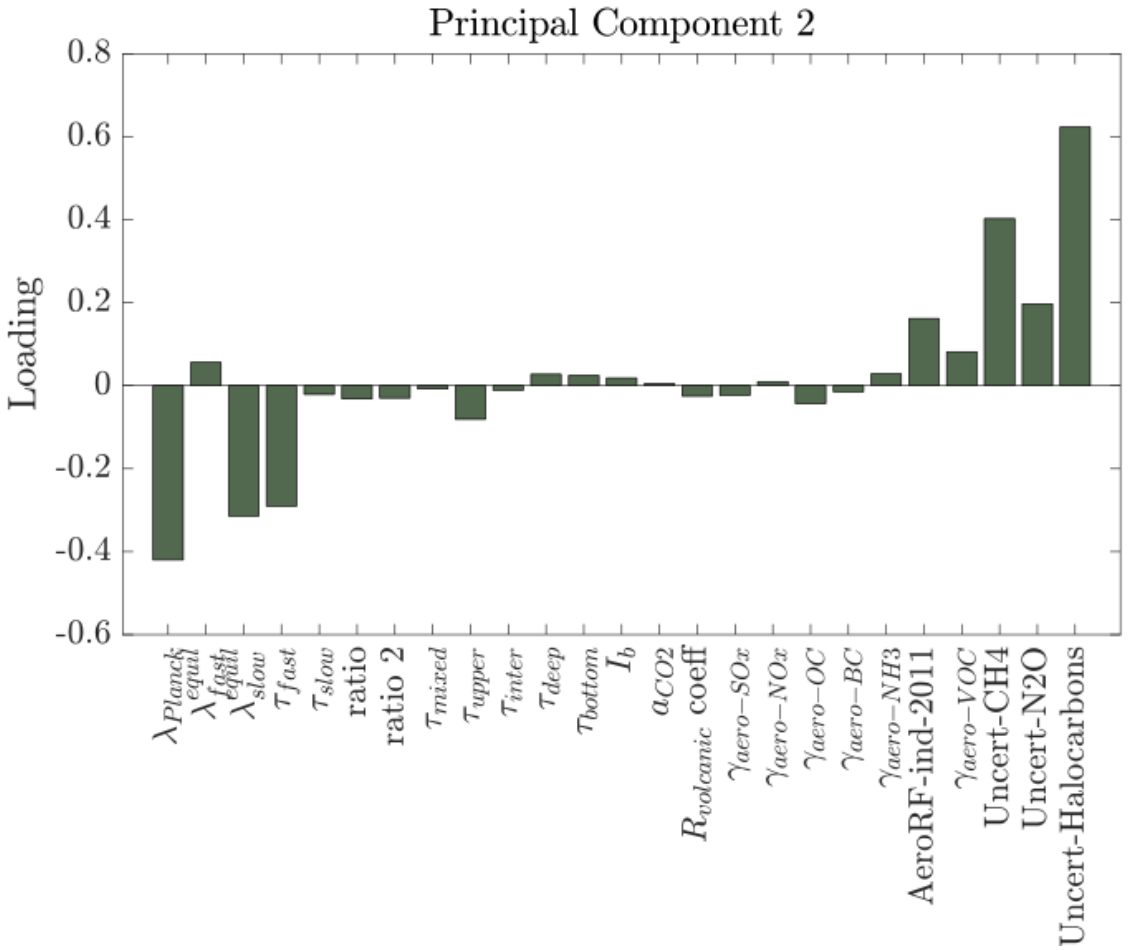

Figure S2. Principle Component 2 of the posterior model ensembles.

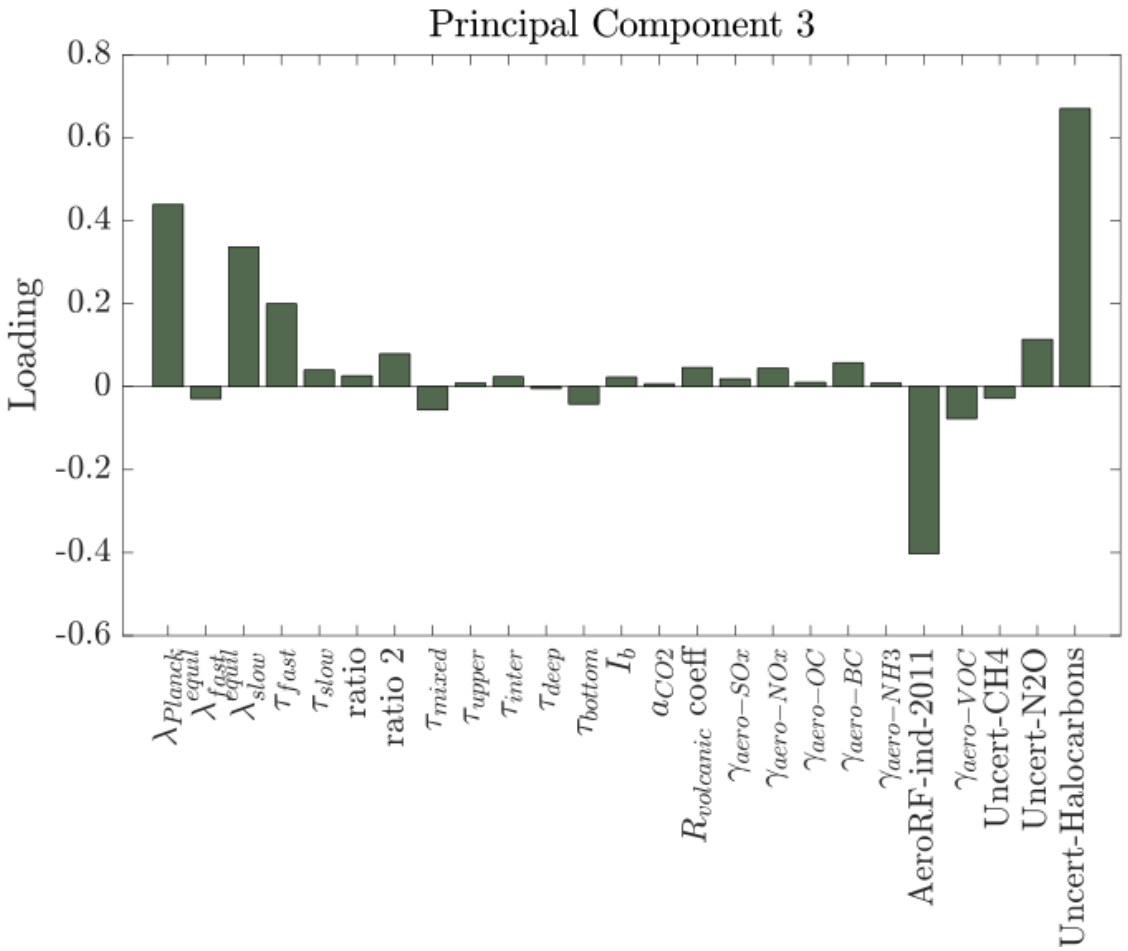

Figure S3. Principle Component 3 of the posterior model ensembles.

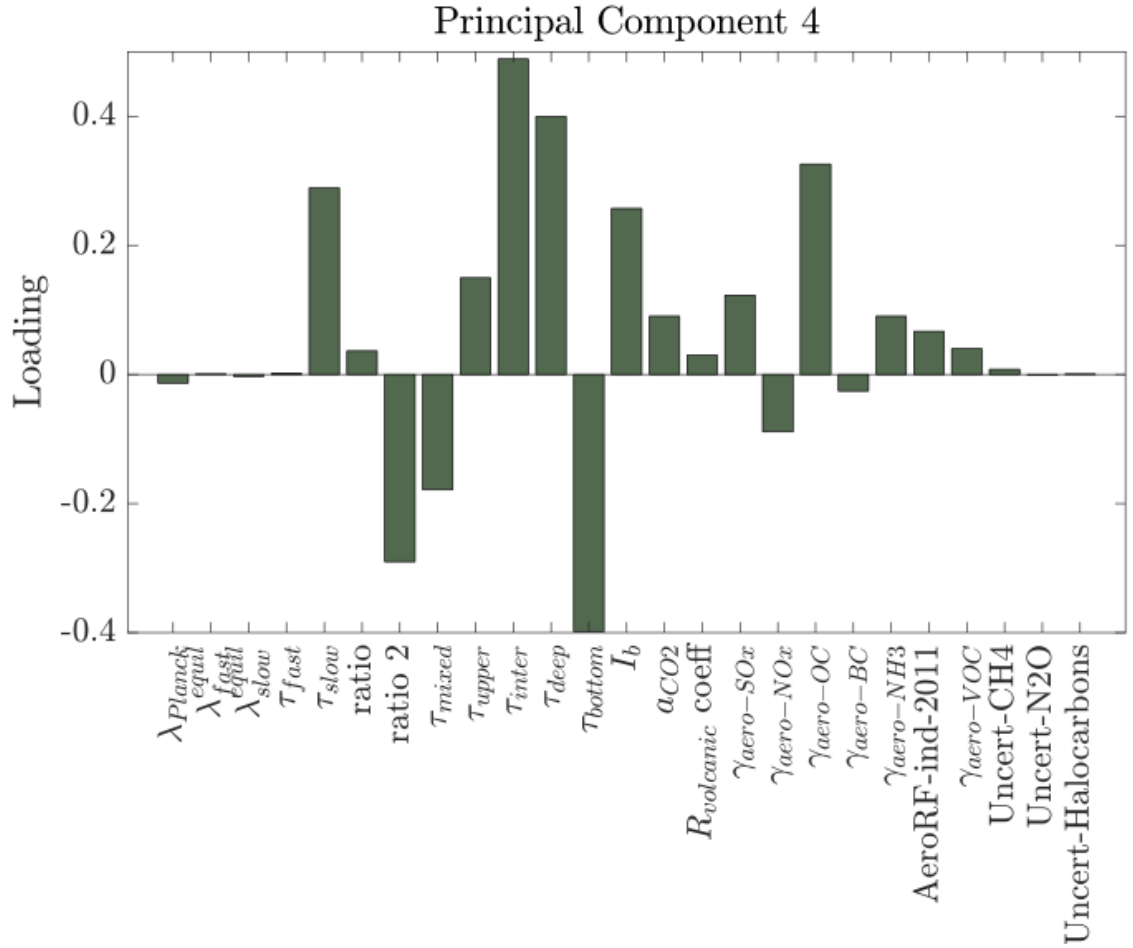

Figure S4. Principle Component 4 of the posterior model ensembles.

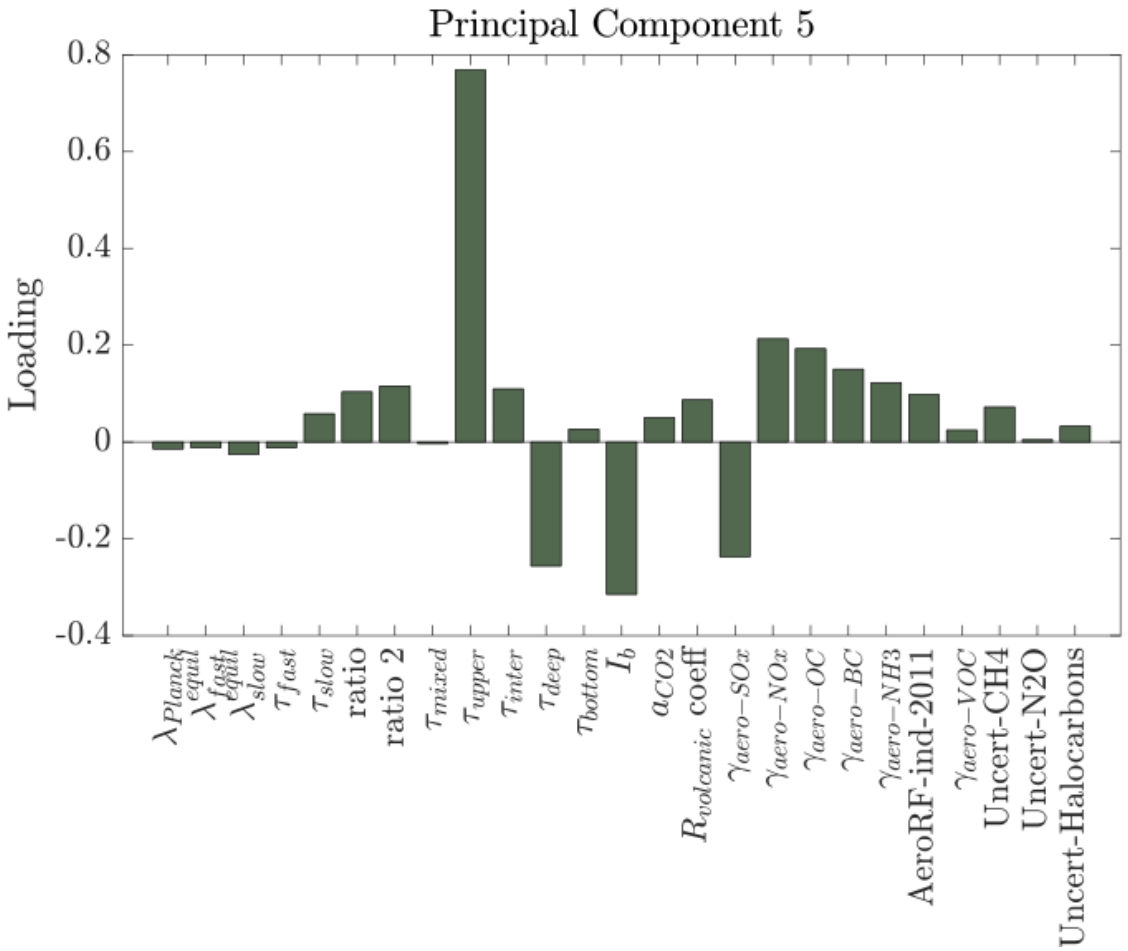

Figure S5. Principle Component 5 of the posterior model ensembles.